PHYSICAL REVIEW D **74,** 034503 (2006)

Landau gauge ghost and gluon propagators in $SU(2)$ lattice gauge theory: Gribov ambiguity reexamined

I. L. Bogolubsky
Joint Institute for Nuclear Research, 141980 Dubna, Russia

G. Burgio and M. Müller-Preussker
Humboldt-Universität zu Berlin, Institut für Physik, 12489 Berlin, Germany

V. K. Mitrjushkin
Joint Institute for Nuclear Research, 141980 Dubna, Russia and Institute of Theoretical and Experimental Physics, Moscow, Russia

(Received 24 November 2005; published 2 August 2006)

We reinvestigate the problem of Gribov ambiguities within the Landau (or Lorentz) gauge for the ghost and gluon propagators in pure $SU(2)$ lattice gauge theory. We make use of the full symmetry group of the action taking into account *large*, i.e. nonperiodic, $\mathbb{Z}(2)$ gauge transformations leaving lattice plaquettes invariant. Enlarging in this way the gauge orbits for any given gauge field configuration the Landau gauge can be fixed at higher local extrema of the gauge functional in comparison with standard (overrelaxation) techniques. This has a clearly visible effect not only for the ghost propagator at small momenta but also for the gluon propagator, in contrast to the common belief.

DOI: 10.1103/PhysRevD.74.034503 PACS numbers: 11.15.Ha, 12.38.Gc, 12.38.Aw

I. INTRODUCTION

It is an important task to compute (Landau or Coulomb) gauge gluon, ghost, and fermion propagators, and the basic vertex functions from nonperturbative approaches to $SU(N)$ gauge theories, like Dyson-Schwinger equations or the lattice formulation. On one hand, one is interested in their behavior in the infrared limit in order to extract nonperturbative information on various observables, e.g. the QCD running couplings $\alpha_s(q^2)$, to understand quark and gluon confinement within the Gribov-Zwanziger scenario [1–3], or to check the Kugo-Ojima confinement criterion for the absence of colored states [4]. On the other hand, it is technically important to see to what extent these different nonperturbative approaches provide results consistent with each other in the nonperturbative region, i.e. at low momenta. At present we are still far from drawing final conclusions in this respect. In particular, the Dyson-Schwinger approach [5–7], always relying on a truncated set of equations, provides results which look quite different in the infinite volume limit compared with those obtained on a torus [8–10], while the latter show at least qualitative agreement with recent results of numerical lattice simulations [11].

It is well known that gauge fixing in the nonperturbative range faces the Gribov ambiguity problem, which means that there can be many gauge copies for a given gauge field satisfying the Landau gauge condition $\partial_\mu A_\mu = 0$ within the Gribov region, the latter defined by the positivity of the Landau gauge Faddeev-Popov operator. In recent years one has checked in greater detail how strong Gribov copies can influence the infrared behavior especially of the gluon and ghost propagators. Several groups of authors came to the conclusion that, while there is a clearly visible influence on the ghost propagator, the gluon propagator seems only weakly affected [11–15].

Recently Zwanziger has argued that in the infinite volume limit the influence of Gribov copies "... might be negligible, i.e. all averages taken over the Gribov region should become equal to averages over the fundamental modular region" [3]. However, in practical lattice simulations we are always restricted to finite volumes. Thus, Gribov copies have to be taken into account properly before extrapolating to the infrared and infinite volumes.

In this paper we present a reinvestigation of the Gribov copy problem for the $SU(2)$ case. The usual way to fix the (Landau) gauge on the lattice is to simulate the path integral in its gauge-invariant form. Subsequently each of the produced lattice gauge fields $U \equiv \{U_{x,\mu}\}$ is subjected to an iterative procedure maximizing the gauge functional

$$F(g) = \frac{1}{dV}\sum_{x,\mu}\frac{1}{2}\,\mathrm{Tr}U^g_{x,\mu}, \qquad U^g_{x,\mu} = g(x)U_{x,\mu}g^\dagger(x+\hat{\mu}) \tag{1}$$

with respect to local gauge transformations $g \equiv \{g(x) \in SU(2)\}$. $V = L^d$ denotes the number of lattice sites in $d = 4$ dimensions. The local maxima of $F(g)$ satisfy the differential lattice Landau gauge transversality condition

$$(\partial_\mu A^g_\mu)(x) = A^g_\mu(x+\hat{\mu}/2) - A^g_\mu(x-\hat{\mu}/2) = 0, \tag{2}$$

where the lattice gauge potentials are

$$A_\mu(x+\hat{\mu}/2) = \frac{1}{2i}(U_{x,\mu} - U^\dagger_{x,\mu}). \tag{3}$$

The standard procedure assumes *periodic gauge transformations* and employs the *overrelaxation algorithm*. In what follows we shall abbreviate it by *SOR*. The influence

of Gribov copies can be easily studied by taking various initial random gauge copies of the gauge field configurations before subjecting them to the SOR algorithm.

At this place it is worth noting that the widely—at least until now—accepted approach to compute e.g. a gauge-variant propagator G is to always choose the gauge copy with the highest value of local maxima $F_{\max}$ [or the *best copy* (bc)] found for the gauge functional (1). One can then hope to have found a copy belonging to the so-called *fundamental modular region* or at least not far from it. In order to find the *best copy* for each thermalized gauge field configuration, one needs to compare $F_{\max}$ values for a pretty large amount of gauge copies, which is a rather time consuming procedure. A reasonable question is if the use of only one gauge copy [the *first copy* (fc)] provides us with the same—within error bars—values of the propagator as the use of the best copy would. This logic brings us to compare the propagator calculated on best copies ($G^{(\mathrm{bc})}$) with that on the first copies ($G^{(\mathrm{fc})}$). The relative deviation $\delta G \equiv |(G^{(\mathrm{fc})} - G^{(\mathrm{bc})})/G^{(\mathrm{bc})}|$ then provides a useful quantitative measure of the Gribov ambiguity of the quantity under consideration. We shall discuss this measure throughout the present paper.

Of course, one can enhance the effect of Gribov copies by comparing instead the best copies with the *worst copies*, i.e. with those having the smallest $F_{\max}$ values found from the repeated use of a given maximization method. This attitude has been taken in Ref. [15] in order to highlight a Gribov copy effect for the gluon propagator.

In Refs. [13] for $SU(2)$ and [11] for $SU(3)$ some of us already have thoroughly discussed the impact of Gribov copies within the SOR framework by comparing first and best copies. From this point of view the gluon propagator did not depend on the copies within the statistical noise, whereas the ghost propagator clearly did depend on them in the infrared. But the data for the ghost propagator obtained for different lattice sizes showed an indication for a weakening of the dependence on the choice of Gribov copies for increasing lattice size at fixed momentum, in agreement with Zwanziger's claim [3].

Here we enlarge the class of possible gauge transformations by also taking into account *nonperiodic* center gauge transformations. This will allow us to further maximize the gauge functional and to see a quite strong Gribov copy effect also for the gluon propagator at finite (lattice) volumes.

In Sec. II we shall explain the improved gauge fixing procedure. In Sec. III we define the propagators to be calculated. In Sec. IV we present our results for the gluon and ghost propagators, whereas in Sec. V the conclusions are drawn.

II. IMPROVED GAUGE FIXING

We shall deal all the time with $SU(2)$ pure gauge lattice fields in four Euclidean dimensions produced by means of Monte Carlo simulations with the standard Wilson plaquette action. We restrict ourselves to the confinement phase at $T = 0$.

To fix the gauge, we employ the standard Los Alamos type overrelaxation with $\omega = 1.7$.

Our generalization of the standard gauge fixing procedure SOR comes from the simple observation that gauge covariance for periodic $SU(2)$ gauge fields on a d-dimensional torus of extension L^d allows gauge transformations which are not necessarily periodic but can differ by a group center element at the boundary:

$$g(x + L\hat{\nu}) = z_\nu g(x), \qquad z_\nu = \pm 1 \in \mathbb{Z}(2). \tag{4}$$

In light of this, it is legitimate to allow, during the maximization of the gauge functional in the gauge fixing procedure, for gauge transformations which differ by a sign when winding around a boundary. Let ν be the direction of such a boundary. Any such gauge transformation can be decomposed into a standard periodic gauge transformation (which we may call a ''small'' one) and a flip of all links $U_\nu(x) \rightarrow -U_\nu(x)$ of a 3-plane at a given fixed x_ν. Given a small random gauge copy of the configuration, we have thus performed a preconditioning step for the gauge functional by sweeping in every direction all 3-planes in succession and comparing the value of the flipped with the unflipped gauge functional. The flip is accepted if the gauge functional increases. It is easy to see that such a procedure is independent of the order of choosing the 3-planes and that only one sweep through the lattice is required to maximize the functional. The gauge copy obtained at the end of this procedure is then used as a starting point for a standard maximization procedure. We call the whole procedure FOR.

Analogously to the SOR method, the FOR procedure can be repeated with different initial random gauges in order to find a best copy, in comparison e.g. with the first random copy. We shall check the convergence of the bc-propagator results for the best copies as a function of the number n_{copy} of random initial copies.

III. GLUON AND GHOST PROPAGATORS

We turn now to the computation of the gauge-variant gluon and ghost propagators within the Landau gauge.

The lattice gluon propagator $D^{ab}_{\mu\nu}(p)$ is taken as the Fourier transform of the gluon two-point function, i.e. the expectation value

$$D^{ab}_{\mu\nu}(p) = \langle \tilde{A}^a_\mu(\hat{k}) \tilde{A}^b_\nu(-\hat{k}) \rangle_U = \delta^{ab} \left(\delta_{\mu\nu} - \frac{p_\mu p_\nu}{p^2} \right) D(p). \tag{5}$$

$\tilde{A}^a_\mu(\hat{k})$ is the Fourier transform of the lattice gauge potential $A^a_\mu(x + \hat{\mu}/2)$. p denotes the four-momentum

$$p_\mu(\hat{k}_\mu) = \frac{2}{a}\sin\left(\frac{\pi\hat{k}_\mu}{L}\right) \tag{6}$$

with the integer-valued lattice momentum $\hat{k}_\mu \in (-L/2, +L/2]$. a is the lattice spacing.

The lattice ghost propagator is defined by inverting the Faddeev-Popov (F-P) operator, the latter being the Hessian of the gauge functional, Eq. (1). The F-P operator can be written in terms of the (gauge-fixed) link variables $U_{x,\mu}$ as

$$M^{ab}_{xy} = \sum_\mu A^{ab}_{x,\mu}\delta_{x,y} - B^{ab}_{x,\mu}\delta_{x+\hat{\mu},y} - C^{ab}_{x,\mu}\delta_{x-\hat{\mu},y} \tag{7}$$

with

$$A^{ab}_{x,\mu} = \tfrac{1}{2}\delta_{ab}\,\mathrm{Tr}[U_{x,\mu} + U_{x-\hat{\mu},\mu}],$$
$$B^{ab}_{x,\mu} = \tfrac{1}{2}\mathrm{Tr}[\sigma^b\sigma^a U_{x,\mu}], \qquad C^{ab}_{x,\mu} = \tfrac{1}{2}\mathrm{Tr}[\sigma^a\sigma^b U_{x-\hat{\mu},\mu}],$$

where the σ^a ($a = 1, 2, 3$) are the Pauli matrices. In the continuum M^{ab}_{xy} corresponds to the operator $M^{ab} = -\partial_\mu D^{ab}_\mu$, with D^{ab} the covariant derivative in the adjoint representation.

The ghost propagator in momentum space is calculated from the ensemble average

$$G^{ab}(p) = \frac{1}{V}\sum_{x,y}\langle e^{-2\pi i\hat{k}\cdot(x-y)}[M^{-1}]^{ab}_{xy}\rangle_U \tag{8}$$

$$= \delta^{ab}G(p). \tag{9}$$

Following Refs. [12,16] we have used the conjugate gradient (CG) algorithm to invert M on a plane wave $\vec{\psi}_c = \{\delta_{ac}\exp(2\pi i\hat{k}\cdot x)\}$.

After solving $M\vec{\phi} = \vec{\psi}_c$ the resulting vector $\vec{\phi}$ is projected back on $\vec{\psi}$ so that the average $G^{cc}(p)$ over the color index c can be taken explicitly. Since the F-P operator M is zero if acting on constant modes, only $\hat{k} \neq (0, 0, 0, 0)$ is permitted. Because of high computational requirements to invert the F-P operator for each $\hat{k}$, separately, the estimators on a single, gauge-fixed configuration are evaluated only for a preselected set of momenta $\hat{k}$.

IV. RESULTS

We consider various bare couplings in the interval $\beta = 4/g_0^2 \in [2.1, 2.5]$ and lattice sizes up to 20^4. We compare the gluon and ghost propagators obtained with the alternative gauge fixing methods SOR ("flips off") and FOR ("flips on") both for the first copy (`fc`) and best copy (`bc`). In order to find the best copies, we always generate 20 initial random gauge copies.

In Fig. 1 we illustrate for the FOR method how fast the gluon and ghost propagators are converging when determined from the best copy out of the first n_{copy} copies. We see plateaus occurring for $n_{\mathrm{copy}} \geq O(10)$. We have convinced ourselves that $O(20)$ copies are sufficient at least for $\beta \geq 2.3$ and lattice sizes up to 20^4. For the SOR method the convergence is faster—although to worse values of the gauge functional—such that, in principle, a smaller number of copies would be sufficient within the given parameter range.

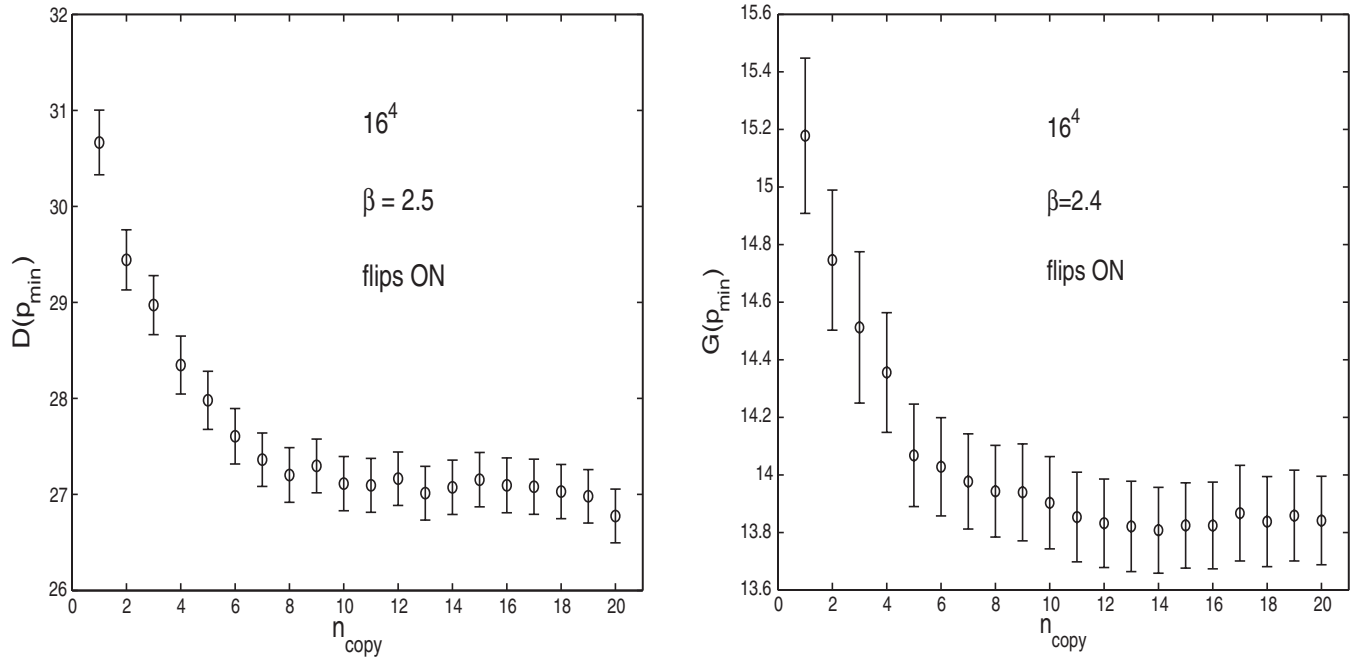

FIG. 1. Gluon propagator (left panel) and ghost propagator (right panel) at lowest momentum $p_{\mathrm{min}} = (2/a)\sin(\pi/L)$ versus the number of random copies employing the FOR method (flips on) at $\beta = 2.5$ and 2.4, respectively (lattice size 16^4).

Mostly, we have concentrated on the lowest nontrivial on-axis lattice momentum $p_{\min} = (2/a)\sin(\pi/L)$ and some multiple on-axis momenta in order to study the infrared limit for a given lattice size and bare coupling. We are aware of the fact that this choice is by far too restrictive to get reliable results for the (renormalized) propagators in the continuum and thermodynamic limits.

In Figs. 2 and 3 we show our results for the lattice gluon $D(p_{\min})$ and ghost propagators $G(p_{\min})$ for 12^4 and 16^4 lattices, always for the smallest nonvanishing momentum. In order to demonstrate the effect of the $\mathbb{Z}(2)$ flips in comparison with the SOR results obtained with `bc` and `fc` [13], we show three sets of data points: black dots correspond to FOR (flips on and `bc` copies) and open

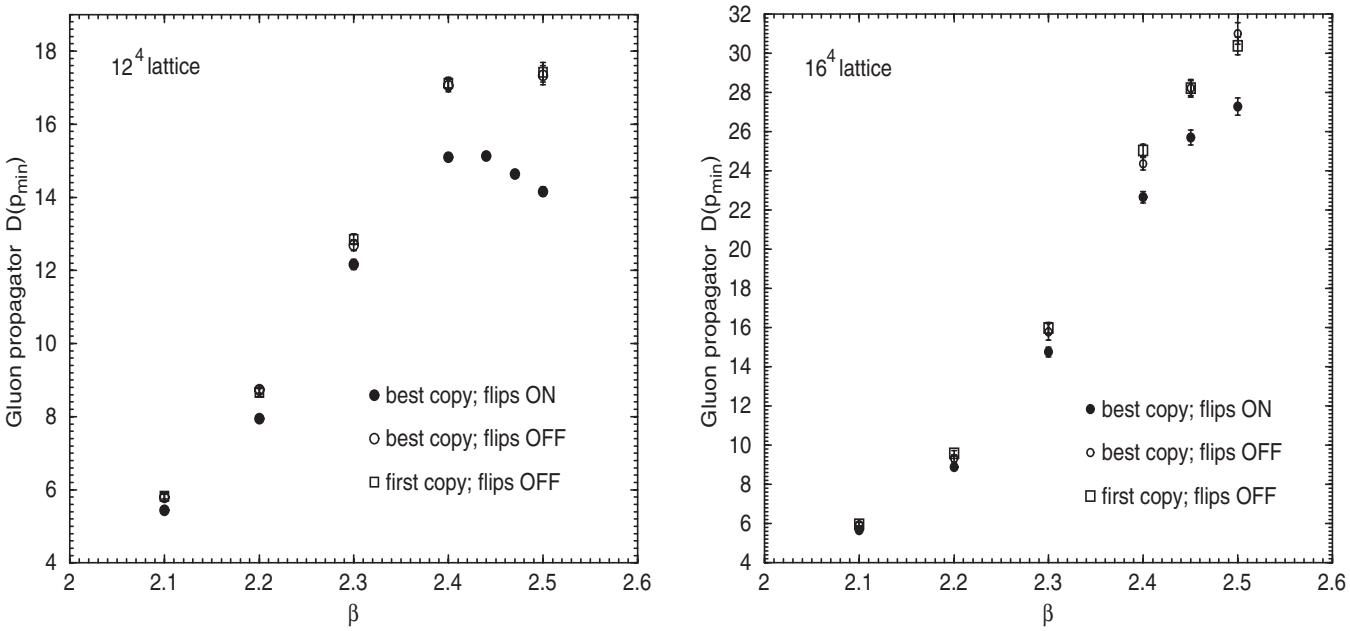

FIG. 2. Gluon propagator $D(p_{\min})$ at lowest momentum for various β and for lattice sizes 12^4 (left panel) and 16^4 (right panel). Full dots refer to FOR `fc` and open squares (circles) correspond to SOR `fc` (`bc`).

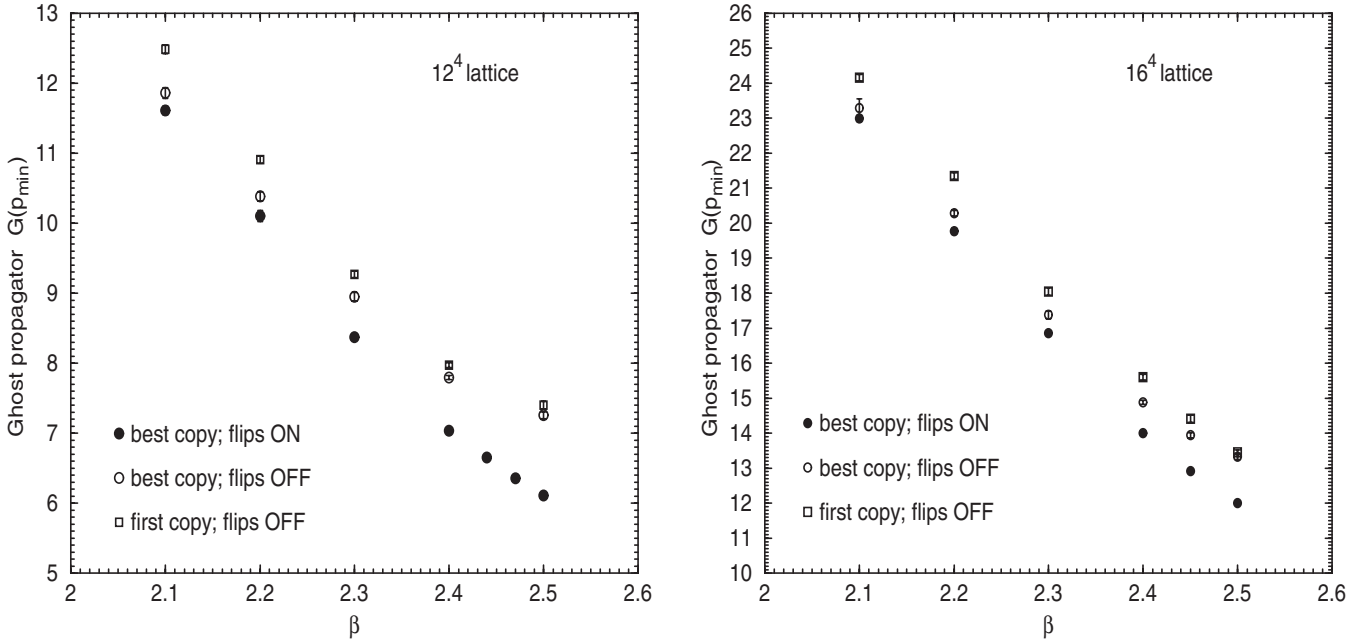

FIG. 3. Ghost propagator $G(p_{\min})$ as for Fig. 2.

circles (squares) correspond to SOR [flips off for bc (fc) copies]. The corresponding data are listed in Table I.

We clearly see that the FOR method leads to an additional visible Gribov copy effect not only for the ghost propagator but also for the gluon propagator. The effect is even more pronounced at higher β values, i.e. at smaller "physical" lattice sizes. We have convinced ourselves that this is compatible with the behavior of the average maximal gauge functional $\langle F_{\max} \rangle$. Its relative difference determined with bc copies for the FOR method versus the SOR method is also rising with β. Later on we shall see that this observation is also in one-to-one correspondence with the gauge copy dependence for fixed β and varying lattice size. The anatomy of the (new) FOR gauge copies deserves further studies in the future.

TABLE I. Data for the gluon propagator $D(p)$ (left) as well as for the ghost propagator $G(p)$ (right) at lowest momentum $p = p_{\min}$ obtained with FOR (bc) and SOR (bc and fc) methods on 12^4 and 16^4 lattices.

			12^4		
β	#	$D^{(bc)}_{FOR}$	#	$D^{(bc)}_{SOR}$	$D^{(fc)}_{SOR}$
2.10	1200	5.39(6)	900	5.79(8)	5.83(8)
2.20	1200	7.94(9)	1200	8.74(10)	8.66(10)
2.30	1200	12.16(14)	1200	12.69(15)	12.85(15)
2.40	3600	15.10(10)	2080	17.06(17)	17.12(17)
2.44	5100	15.13(9)			
2.47	5700	14.64(9)			
2.50	2650	14.16(13)	1760	17.34(26)	17.42(26)
			16^4		
β	#	$D^{(bc)}_{FOR}$	#	$D^{(bc)}_{SOR}$	$D^{(fc)}_{SOR}$
2.10	1042	5.59(7)	918	5.93(8)	5.95(8)
2.20	900	9.01(12)	740	9.35(14)	9.58(14)
2.30	1100	14.88(18)	510	16.16(31)	15.97(29)
2.40	1032	22.65(29)	1020	24.36(32)	25.03(32)
2.45	1020	25.69(32)	1030	28.19(36)	28.21(38)
2.50	1040	26.86(35)	1060	30.64(44)	30.37(45)

			12^4		
β	#	$G^{(bc)}_{FOR}$	#	$G^{(bc)}_{SOR}$	$G^{(fc)}_{SOR}$
2.10	1200	11.58(4)	900	11.87(4)	12.48(7)
2.20	1200	10.10(8)	1200	10.39(3)	10.90(5)
2.30	1200	8.37(2)	1200	8.99(6)	9.27(4)
2.40	3600	7.04(1)	2080	7.80(3)	7.97(4)
2.44	5100	6.65(1)			
2.47	5700	6.36(1)			
2.50	2650	6.11(1)	1760	7.26(5)	7.40(5)
			16^4		
β	#	$G^{(bc)}_{FOR}$	#	$G^{(bc)}_{SOR}$	$G^{(fc)}_{SOR}$
2.10	1042	22.89(6)	918	23.12(13)	24.15(8)
2.20	900	19.83(6)	740	20.29(6)	21.34(9)
2.30	1100	16.83(5)	510	17.27(8)	18.05(10)
2.40	1032	14.00(4)	1020	14.88(6)	15.60(8)
2.45	1020	12.92(5)	1030	13.86(6)	14.41(11)
2.50	1040	12.02(4)	1060	13.26(6)	13.45(7)

In order to illustrate the strong Gribov copy effect in a slightly different manner, we compare smoothed distributions for the mean value estimators for the gluon and ghost propagators for the bc with the FOR and SOR methods, respectively (see Fig. 4). The mean value distributions have been obtained in accordance with the bootstrap method [17] from replica of sequences of randomly selected data. Such bootstrapped resampling was applied to the initial Monte-Carlo data set as a whole, the amount of replicas being typically 200. To smooth the distribution we have used the standard Nadaraya-Watson method with normal kernel [18], and an improved Silverman's rule of thumb for the choice of the corresponding bandwidth.

It is worth mentioning that the statistical errors for most of our data have also been estimated through bootstrapped resampling.

We have also studied how the Gribov copy effect develops for larger momenta $p(\hat{k})$. We have used multiples of the minimal lattice momentum $\hat{k} = (0, 0, 0, k)$ $(k = 1, 2, 3, 4)$ along one axis. We compare for the gluon propagator the bc SOR results with the bc FOR results in terms of the relative deviation

$$\delta D(p) = (D^{(bc)}_{SOR} - D^{(bc)}_{FOR})/D^{(bc)}_{FOR}, \qquad (10)$$

and analogously for the ghost propagator $G(p)$ at various β values and with fixed lattice size 16^4 (see Fig. 5). For the gluon propagator our results are restricted to only one β value because of the much stronger statistical noise. Nevertheless, the results presented for the gluon propagator point in the same direction as for the ghost propagator. The effect of Gribov copies still remains noticeable at $p > p_{\min}$, although decreasing for rising momenta. The data for the ghost propagator at various momenta obtained from independent Monte Carlo runs are also collected in Table II.

We have also made a corresponding check for the gluon propagator at zero momentum. On a lattice of size 20^4 and for the same $\beta = 2.5$, we observed a deviation between the bc FOR and SOR results of the order $O(25\%)$. This would, of course, have consequences for estimates like in Refs. [19,20], since the infinite volume extrapolation of $D(0)$ performed there, although probably remaining finite, will definitely suffer from uncontrolled systematic uncertainties.

It is interesting to study the volume dependence of the Gribov copy effect, in view of Zwanziger's recent claim mentioned at the beginning [3]. First of all, we have convinced ourselves that the number of gauge copies is strongly rising with the lattice volume as it should be. This is clearly demonstrated in Fig. 6, providing the distributions of the number of gauge copies per configuration found with the FOR method (flips on) for lattice sizes 8^4 and 16^4 at $\beta = 2.40$. In both cases we have generated 100

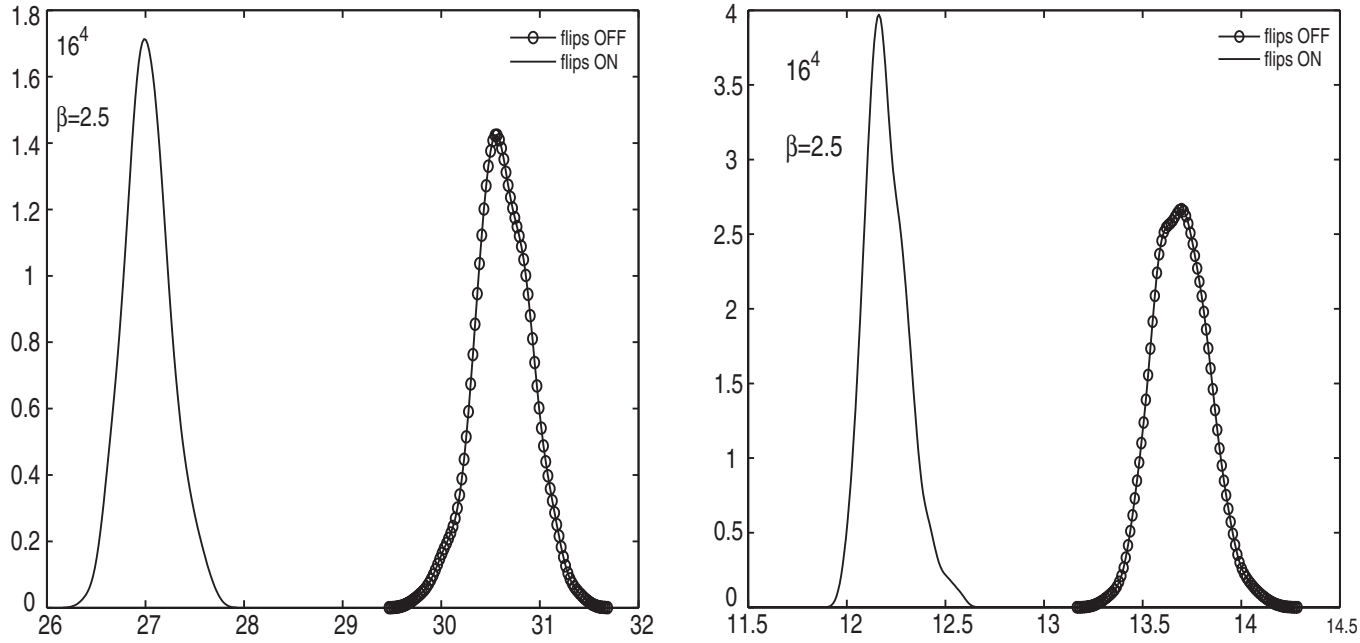

FIG. 4. SOR and FOR distributions for $D^{(\mathrm{bc})}(p_{\min})$ (left panel) and $G^{(\mathrm{bc})}(p_{\min})$ (right panel) at $\beta = 2.5$ and 16^4 lattices.

configurations with 100 gauge copies each. It turns out that identical (or degenerated) copies can be well recognized at an accuracy for the gauge functional, Eq. (1), of $O(10^{-10})$. Adjacent copies normally differ in the values for the gauge functional at a level of $O(10^{-6})$. Now let us compare the distributions of the corresponding values of the functional F for each copy found. In order to normalize the values with respect to the highest (i.e. best) value per configuration, we show the relative deviation $(F^{(\mathrm{bc})}_{\max} - F_{\max})/F^{(\mathrm{bc})}_{\max}$. The frequency distributions of these values are shown in Fig. 7 for the same ensembles as used for Fig. 6. There is a very clear tendency that the variance of the gauge func-

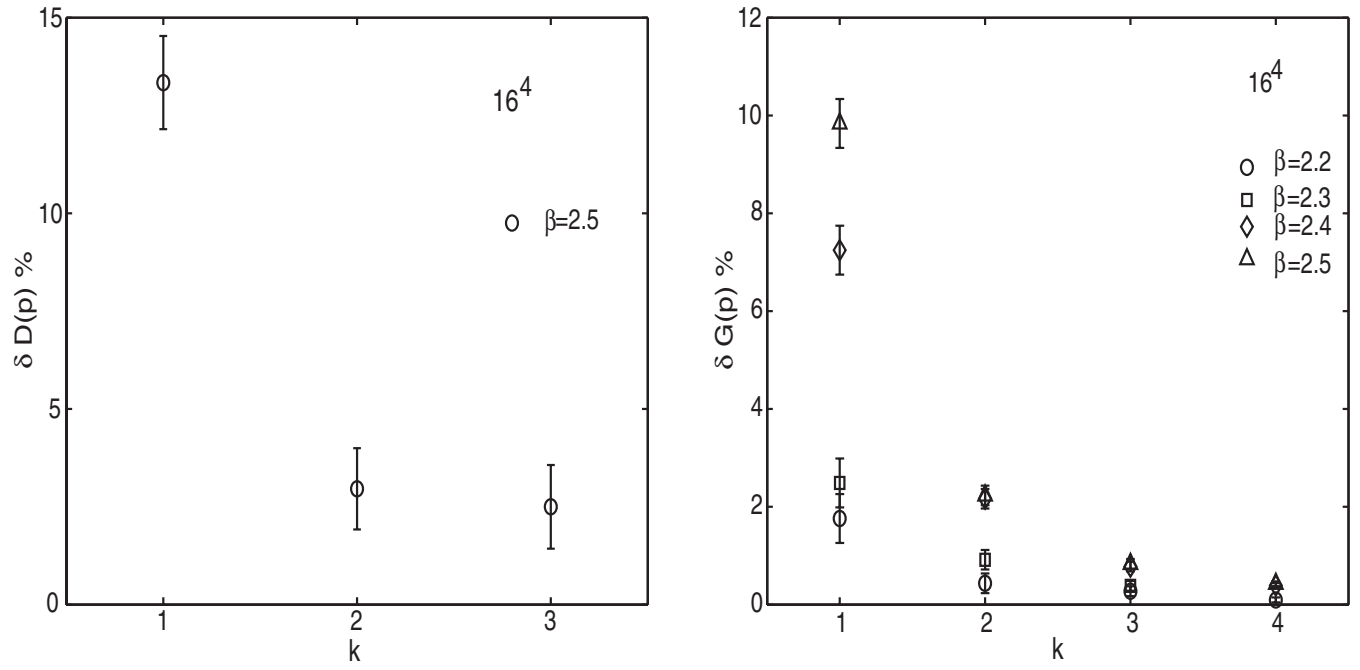

FIG. 5. Left panel: relative deviation $\delta D(p) = (D^{(\mathrm{bc})}_{\mathrm{SOR}} - D^{(\mathrm{bc})}_{\mathrm{FOR}})/D^{(\mathrm{bc})}_{\mathrm{FOR}}$ in percent for the gluon propagator at various (on-axis) lattice momenta $p(k)$ (lattice size 16^4, $\beta = 2.5$). Right panel: the analogous relative deviation for the ghost propagator for the same lattice size but for $\beta = 2.2$, 2.3, 2.4, and 2.5.

TABLE II. Ghost propagators $G(p)$ on the 16^4 lattice for various on-axis lattice momenta $p(k)$.

β	#		$G(k=1)$	$G(k=2)$	$G(k=3)$	$G(k=4)$
			FOR			
2.20	400	fc	21.2(1)	3.96(1)	1.510(2)	0.8116(5)
		bc	19.88(8)	3.868(7)	1.493(1)	0.8076(4)
2.30	400	fc	18.2(2)	3.39(3)	1.313(2)	0.7276(6)
		bc	16.88(8)	3.267(6)	1.299(1)	0.7241(4)
2.40	356	fc	15.4(1)	2.87(1)	1.171(1)	0.6693(3)
		bc	13.8(1)	2.770(8)	1.156(2)	0.6647(4)
2.50	400	fc	13.7(1)	2.578(5)	1.0897(8)	0.6357(2)
		bc	12.2(1)	2.508(5)	1.079(1)	0.6325(3)
			SOR			
β	#		$G(k=1)$	$G(k=2)$	$G(k=3)$	$G(k=4)$
2.20	200	fc	21.2(2)	3.97(2)8	1.511(3)	0.8117(7)
		bc	20.23(12)	3.885(10)	1.4971(25)	0.8084(7)
2.30	200	fc	18.2(1)	3.35(1)	1.312(2)	0.7272(5)
		bc	17.3(1)	3.297(8)	1.304(1)	0.7253(5)
2.40	370	fc	15.6(1)	2.87(1)	1.171(1)	0.6690(3)
		bc	14.8(1)	2.83(1)	1.165(1)	0.6673(3)
2.50	200	fc	14.1(2)	2.586(8)	1.090(1)	0.6359(4)
		bc	13.4(1)	2.564(6)	1.088(1)	0.6352(3)

tional becomes much smaller if we increase the lattice volume. A similar tendency becomes visible in Fig. 8, where we plot for the same set of configurations and gauge copies the distributions for the single values of the ghost propagator for the lowest nonvanishing on-axis momentum. Also, in this case we have normalized the single

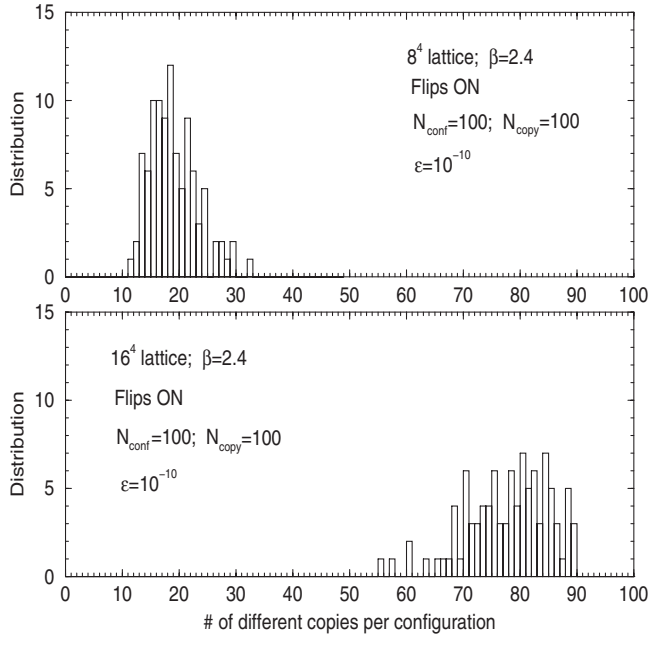

FIG. 6. Distributions of the number of different gauge copies found with the FOR method at $\beta = 2.40$ for lattice sizes 8^4 and 16^4.

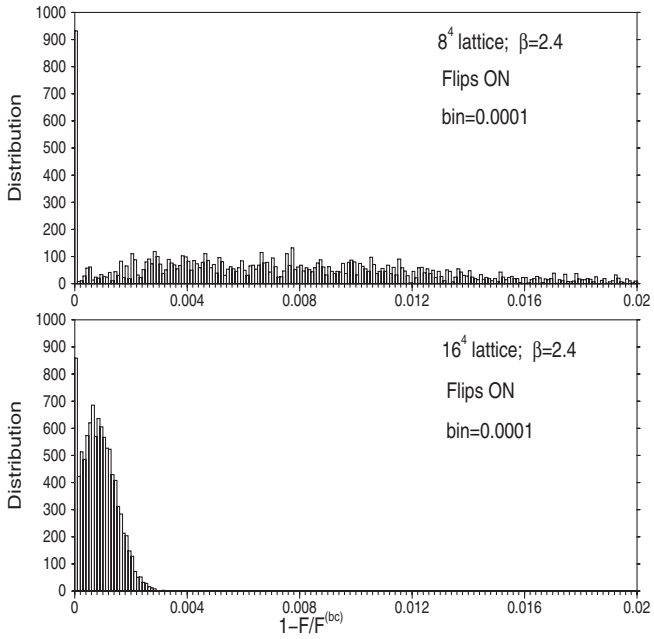

FIG. 7. Distributions of the deviation of the gauge functional values for different gauge copies relative to the best copy per configuration. FOR method at $\beta = 2.40$ for lattice sizes 8^4 and 16^4.

values as $(G^{(\mathrm{bc})} - G)/G^{(\mathrm{bc})}$, i.e. taking the relative deviation of the propagator at a given copy G from the value computed on the best copy G^{bc}, the latter chosen again with respect to the gauge functional value. We see that the long tail seen for the smaller lattice disappears for the larger lattice. Although the fact that close values of the

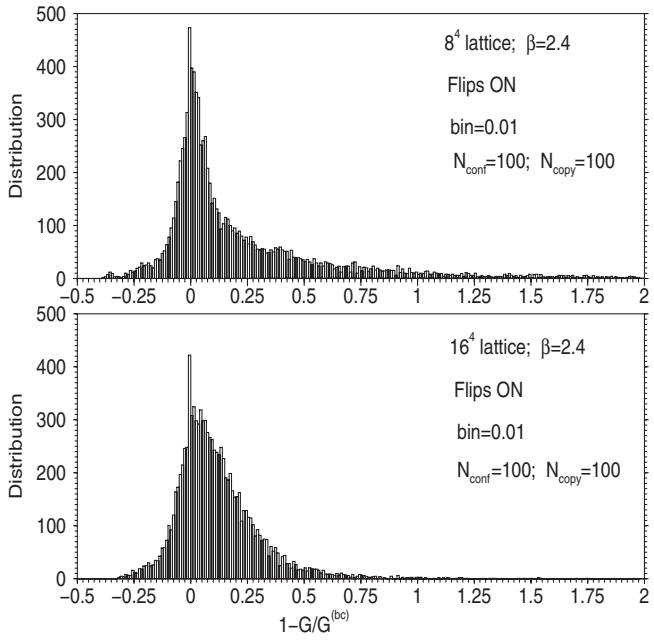

FIG. 8. Distributions of ghost propagator values at lowest nontrivial momentum for different gauge copies as in Fig. 7.

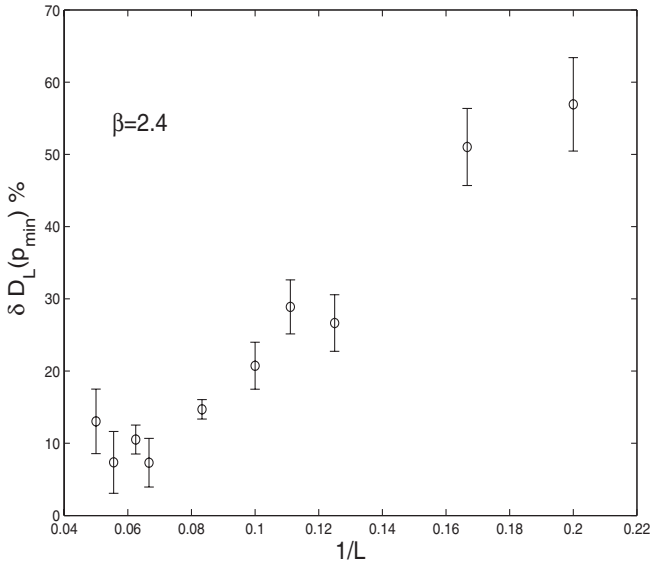

FIG. 9. Relative deviation $\delta D_L(p_{\min}) \equiv (D^{(\mathrm{fc})}_{\mathrm{SOR}} - D^{(\mathrm{bc})}_{\mathrm{FOR}})/D^{(\mathrm{bc})}_{\mathrm{FOR}}$ in percent for the gluon propagator D for various linear lattice sizes L and smallest nonvanishing momentum $p_{\min} = (2/a)\sin(\pi/L)$ ($\beta = 2.4$).

gauge functional will not tell anything about how much the corresponding gauge configurations are differing from each other (irrespective of a global relative gauge transformation), we would like to interpret our finding of shrinking distributions as a weakening of the Gribov problem with increasing physical lattice size.

Moreover, we have plotted the relative deviation

$$\delta D_L(p_{\min}) \equiv (D^{(\mathrm{fc})}_{\mathrm{SOR}} - D^{(\mathrm{bc})}_{\mathrm{FOR}})/D^{(\mathrm{bc})}_{\mathrm{FOR}} \tag{11}$$

for the gluon propagator (see Fig. 9) and analogously for the ghost propagator (see left-hand side of Fig. 10) as a function of the inverse linear lattice size $1/L$, both determined at the minimal momentum $p_{\min}$. Here we have used data for fixed $\beta = 2.4$ and lattice sizes from $L = 5$ up to $L = 20$. In close correspondence to our observations presented in Figs. 2 and 3, we see that the Gribov copy effect becomes weaker (stronger) for increasing (decreasing) physical lattice size and correspondingly decreasing (increasing) minimal momentum, at least up to a certain value of the lattice size ($\lesssim 15$). One would of course need larger values of L to make a reliable conclusion about the limit $L \to \infty$. Anyway, at our largest lattice value $L = 20$ the Gribov copy effect is still quite strong.

For the ghost propagator, where the signal to noise ratio is more favorable, we have also found an analogous behavior for the multiple on-axis momenta $k = 2, 3, 4$ (see right-hand side of Fig. 10).

In [13] two of us have reported on rare Monte Carlo events with exceptionally large values of the ghost propagator occurring for the SOR gauge fixing method for larger β values. In Fig. 11 we show some time histories for the gluon and ghost propagators for $\beta = 2.5$ and a 16^4 lattice, comparing bc SOR with bc FOR. We see that for the "best-copy–flips-on" case (FOR) the fluctuations for both propagators are smaller. But for the ghost propagator the

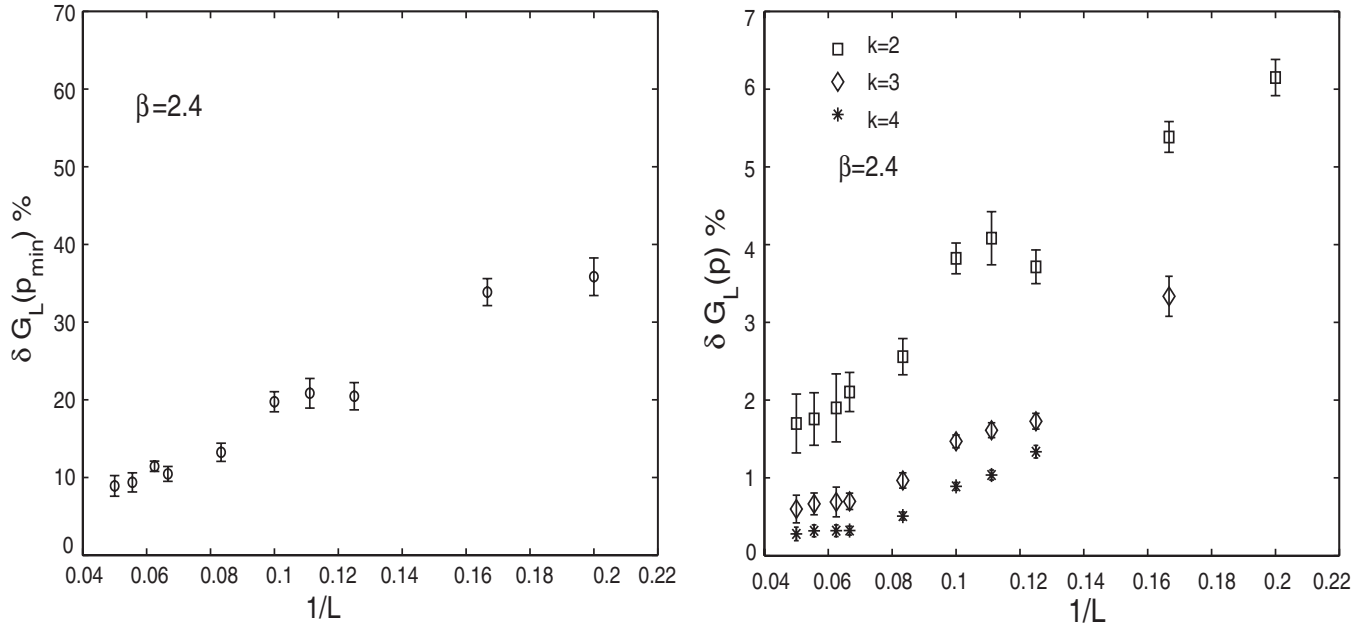

FIG. 10. Relative deviation $\delta G_L(p) \equiv (G^{(\mathrm{fc})}_{\mathrm{SOR}} - G^{(\mathrm{bc})}_{\mathrm{FOR}})/G^{(\mathrm{bc})}_{\mathrm{FOR}}$ in percent for the ghost propagator G at $\beta = 2.4$ for various linear lattice sizes L and the smallest nonvanishing momentum $p_{\min} = (2/a)\sin(\pi/L)$ (left panel) as well as for on-axis momenta $p(k)$ ($k = 2, 3, 4$) (right panel).

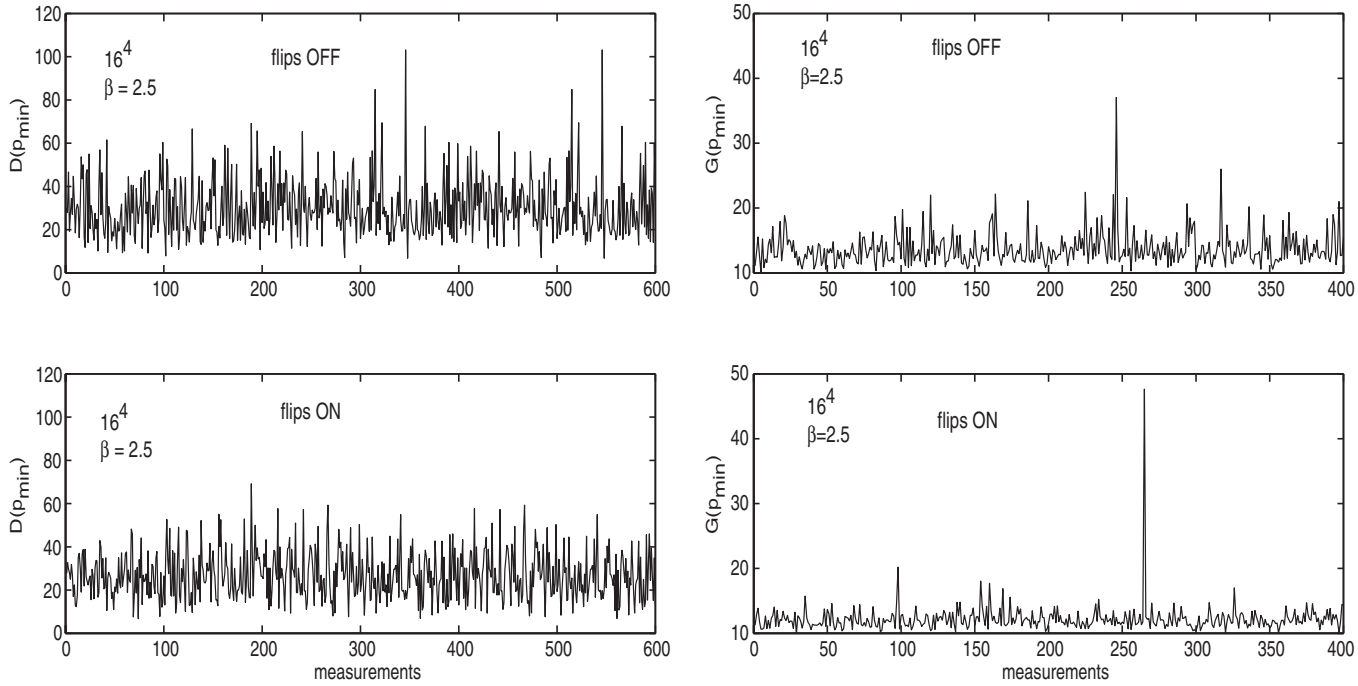

FIG. 11. Time histories for $D^{(bc)}(p_{min})$ (left panel) and $G^{(bc)}(p_{min})$ (right panel) for both SOR and FOR methods at $\beta = 2.5$ and 16^4 lattices.

effect of exceptionally large values, in general related to small eigenvalues of the F-P operator [21], is still there.

In conclusion, we show the form factors of the gluon propagator $p^2D(p)$ and of the ghost propagator $p^2G(p)$ in physical units as a function of the physical momentum for fixed $\beta = 2.4$ and lattice sizes varying from 10^4 to 20^4. We have rescaled the gluon propagator values $D(p)$ with factors a^2 and g_0^2 and the ghost propagator $G(p)$ with a^2, respectively, in order to translate to the corresponding continuum (bare) propagators (compare with [22]). To

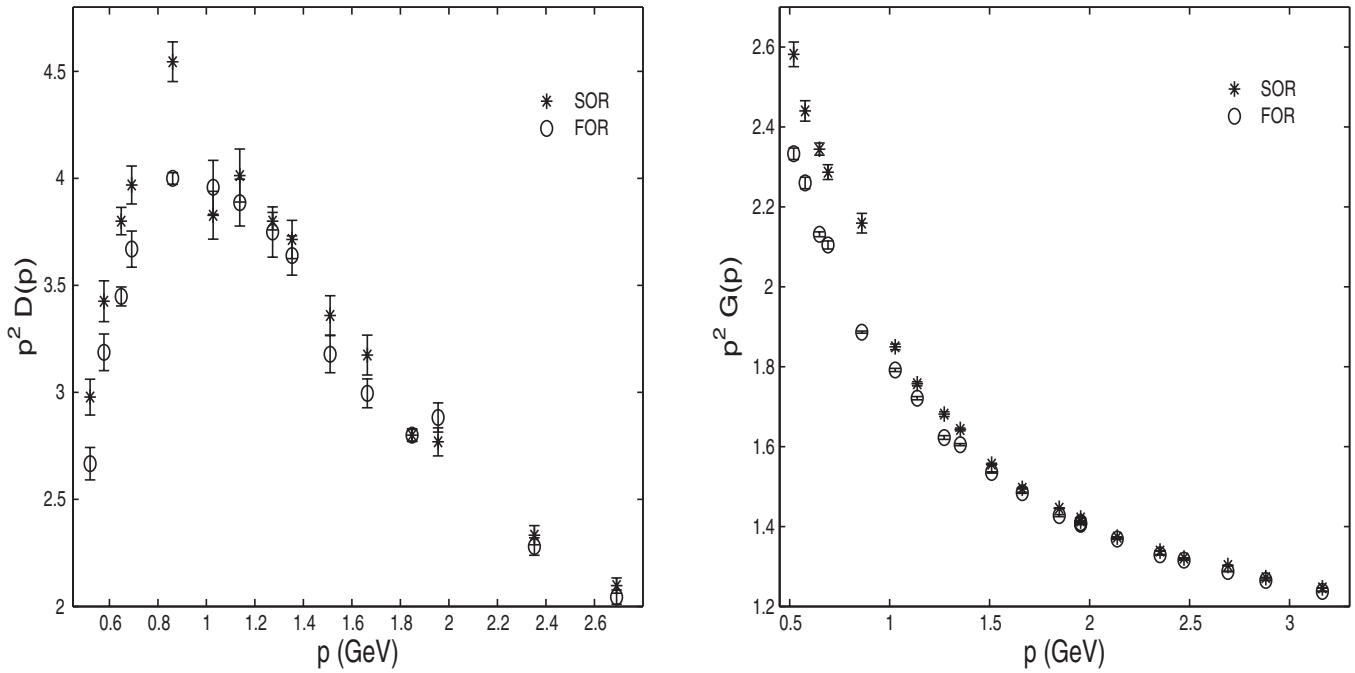

FIG. 12. Gluon form factor $p^2D(p)$ (left panel) and ghost form factor $p^2G(p)$ (right panel) for both the bc SOR and bc FOR methods versus momentum obtained for various lattice sizes and fixed $\beta = 2.4$.

TABLE III. Statistics for the measurements at different L and $\beta = 2.4$.

					FOR					
L	5	6	8	9	10	12	15	16	18	20
N_{conf}	1000	1000	800	600	600	500	400	356	200	200
					SOR					
L	5	6	8	9	10	12	15	16	18	20
N_{conf}	1000	1000	800	500	500	400	400	370	100	100

estimate the lattice spacing in physical units we have used the string tension: $a^2\sigma = .071$ [23] with the standard value $\sqrt{\sigma} = 440$ MeV. The form factor results for both methods bc SOR and bc FOR are shown together in Fig. 12. Again, the figure shows clear Gribov copy effects for both the propagators, not only for the ghost propagator. We did not apply any overall renormalization here. The statistics collected for these runs is listed in Table III.

V. CONCLUSIONS

In this paper we have demonstrated that there is a visible Gribov problem for the ghost propagator as well as for the gluon propagator computed in $SU(2)$ lattice gauge theory within the Landau gauge. In order to show this, we have enlarged the gauge orbits of given Monte Carlo generated gauge fields by nonperiodic $\mathbb{Z}(2)$ transformations, flipping all links in a given direction on a slice orthogonal to that. This allows a preconditioning which maximizes the gauge functional before applying the overrelaxation algorithm.

We have found indications for a weakening of the Gribov copy effect both by going to larger momenta at fixed volume and also by increasing the lattice size L while correspondingly lowering the minimal nonzero momentum, at least up to a certain value of the lattice size ($\lesssim$ 15). However, one would need larger values of L to draw a reliable conclusion about the limit $L \to \infty$.

We have not shown the momentum scheme running coupling which can be determined from the form factors of the propagators discussed here, assuming that the renormalization factor for the ghost-gluon vertex is constant. This will be discussed in a future paper, where we want to present data for larger lattices and a larger spectrum of (off-axis) momenta.

ACKNOWLEDGMENTS

This investigation has been supported by the Heisenberg-Landau program of the collaboration between the Bogoliubov Lab of Theoretical Physics of the Joint Institute for Nuclear Research Dubna, Russia and German institutes. V. K. M. acknowledges support by RFBR Grant No. 05-02-16306. G. B. acknowledges support from INFN. M. M.-P. thanks the DFG for support under Grant No. FOR 465/Mu932/2-2.

[1] V. N. Gribov, Nucl. Phys. **B139**, 1 (1978).
[2] D. Zwanziger, Nucl. Phys. **B412**, 657 (1994).
[3] D. Zwanziger, Phys. Rev. D **69**, 016002 (2004).
[4] T. Kugo and I. Ojima, Prog. Theor. Phys. Suppl. **66**, 1 (1979).
[5] R. Alkofer and L. von Smekal, Phys. Rep. **353**, 281 (2001).
[6] C. S. Fischer and R. Alkofer, Phys. Rev. D **67**, 094020 (2003).
[7] C. Lerche and L. von Smekal, Phys. Rev. D **65**, 125006 (2002).
[8] C. S. Fischer, R. Alkofer, and H. Reinhardt, Phys. Rev. D **65**, 094008 (2002).
[9] C. S. Fischer and R. Alkofer, Phys. Lett. B **536**, 177 (2002).
[10] C. S. Fischer, B. Grüter, and R. Alkofer, Ann. Phys. (N.Y.) **321**, 1918 (2006).
[11] A. Sternbeck, E.-M. Ilgenfritz, M. Müller-Preussker, and A. Schiller, Phys. Rev. D **72**, 014507 (2005).
[12] A. Cucchieri, Nucl. Phys. **B508**, 353 (1997).
[13] T. D. Bakeev, E.-M. Ilgenfritz, V. K. Mitrjushkin, and M. Müller-Preussker, Phys. Rev. D **69**, 074507 (2004).
[14] H. Nakajima and S. Furui, Nucl. Phys. B, Proc. Suppl. **129**, 730 (2004).
[15] P. J. Silva and O. Oliveira, Nucl. Phys. **B690**, 177 (2004).
[16] H. Suman and K. Schilling, Phys. Lett. B **373**, 314 (1996).
[17] B. Efron and R. J. Tibshirani, *An Introduction to the Bootstrap* (Chapman & Hall, London, 1993).
[18] A. W. Bowman and A. Azzalini, *Applied Smoothing Techniques for Data Analysis: The Kernel Method* (Oxford University Press, New York, 1997).
[19] F. D. R. Bonnet, P. O. Bowman, D. B. Leinweber, A. G. Williams, and J. M. Zanotti, Phys. Rev. D **64**, 034501 (2001).
[20] P. Boucaud *et al.*, hep-lat/0602006.
[21] A. Sternbeck, E. M. Ilgenfritz, and M. Müller-Preussker, Phys. Rev. D **73**, 014502 (2006).
[22] J. C. R. Bloch, A. Cucchieri, K. Langfeld, and T. Mendes, Nucl. Phys. **B687**, 76 (2004).
[23] J. Fingberg, U. M. Heller, and F. Karsch, Nucl. Phys. **B392**, 493 (1993).